

Cerium oxide nanoparticles loaded nanofibrous membranes promote bone regeneration for periodontal tissue engineering

Shuangshuang Ren^{a,b,c}, Yi Zhou^{a,b,c}, Kai Zheng^g, Xuanwen Xu^{a,b,c}, Jie Yang^d, Xiaoyu Wang^{e,f},
Leiyang Miao^{d,**}, Hui Wei^{e,f,***}, Yan Xu^{a,b,c,*}

^a Jiangsu Province Key Laboratory of Oral Diseases, Nanjing Medical University, Nanjing, 210029, China

^b Department of Periodontology, The Affiliated Stomatological Hospital of Nanjing Medical University, Nanjing, 210029, China

^c Jiangsu Province Engineering Research Center of Stomatological Translational Medicine, Nanjing 210029, China

^d Nanjing Stomatological Hospital, Medical School of Nanjing University, Nanjing, 210093, China

^e Department of Biomedical Engineering, College of Engineering and Applied Sciences, Nanjing National Laboratory of Microstructures, Jiangsu Key Laboratory of Artificial Functional Materials, Nanjing University, Nanjing, Jiangsu, 210023, China

^f State Key Laboratory of Analytical Chemistry for Life Science, School of Chemistry and Chemical Engineering, Chemistry and Biomedicine Innovation Center (ChemBIC), Nanjing University, Nanjing, Jiangsu 210023, China

^g Institute of Biomaterials, University of Erlangen-Nuremberg, Erlangen, 91058, Germany

ARTICLE INFO

Keywords:

CeO₂ nanoparticles
Periodontal ligament stem cells
Bone regeneration
Electrospinning
Fibrous membrane

ABSTRACT

Bone regeneration is a crucial part in the treatment of periodontal tissue regeneration, in which new attempts come out along with the development of nanomaterials. Herein, the effect of cerium oxide nanoparticles (CeO₂ NPs) on the cell behavior and function of human periodontal ligament stem cells (hPDLSCs) was investigated. Results of CCK-8 and cell cycle tests demonstrated that CeO₂ NPs not only had good biocompatibility, but also promoted cell proliferation. Furthermore, the levels of alkaline phosphatase activity, mineralized nodule formation and expressions of osteogenic genes and proteins demonstrated CeO₂ NPs could promote osteogenesis differentiation of hPDLSCs. Then we chose electrospinning to fabricate fibrous membranes containing CeO₂ NPs. We showed that the composite membranes improved mechanical properties as well as realized release of CeO₂ NPs. We then applied the composite membranes to *in vivo* study in rat cranial defect models. Micro-CT and histopathological evaluations revealed that nanofibrous membranes with CeO₂ NPs further accelerated new bone formation. Those exciting results demonstrated that CeO₂ NPs and porous membrane contributed to osteogenic ability, and CeO₂ NPs contained electrospun membrane may be a promising candidate material for periodontal bone regeneration.

1. Introduction

Periodontitis, a chronic inflammatory disease, results in not only tissue defects including alveolar bone, gingiva, periodontal ligament and cementum, but also system diseases such as adverse pregnancy outcomes, rheumatoid arthritis, Alzheimer's disease and cancer [1–3]. The ultimate goal of periodontal regenerative treatment is to reconstruct the periodontal complex with both hard and soft tissues, in which the alveolar bone is an indispensable part. In clinical practice, guided tissue

regeneration (GTR) and guided bone regeneration (GBR) are two important regeneration approaches to restore functional bone tissues, which can be used alone or in combination with artificial/autogenous bone graft. Most commonly, the GTR/GBR membranes were used to prevent the infiltration of fibrous tissue during periodontal and alveolar bone regeneration [4]. While commercial resorbable barrier membranes have been used for single-step surgical regeneration procedures in clinical, they still have limitations such as high cost, poor mechanical property, improper biodegradation, and unpredictable clinical

Peer review under responsibility of KeAi Communications Co., Ltd.

* Corresponding author. Department of Periodontology, The Affiliated Stomatological Hospital of Nanjing Medical University, Nanjing, 210029, China

** Corresponding author. Nanjing Stomatological Hospital, Medical School of Nanjing University, Nanjing, 210093, China

*** Corresponding author. Department of Biomedical Engineering, College of Engineering and Applied Sciences, Nanjing National Laboratory of Microstructures, Jiangsu Key Laboratory of Artificial Functional Materials, Nanjing University, Nanjing, Jiangsu, 210023, China.

E-mail addresses: miaoleiyang80@163.com (L. Miao), weihui@nju.edu.cn (H. Wei), yanxu@njmu.edu.cn (Y. Xu).

<https://doi.org/10.1016/j.bioactmat.2021.05.037>

Received 22 January 2021; Received in revised form 19 April 2021; Accepted 25 May 2021

Available online 5 June 2021

2452-199X/© 2021 The Authors. Publishing services by Elsevier B.V. on behalf of KeAi Communications Co. Ltd. This is an open access article under the CC

BY-NC-ND license (<http://creativecommons.org/licenses/by-nc-nd/4.0/>).

outcomes especially in horizontal periodontal bone defects [5]. Therefore, the development of artificial biodegradable membranes with low cost, unique structures, proper physicochemical properties and biological ability to achieve more satisfactory tissue regeneration attract increasing attention recently [6–8].

Electrospinning is an effective way to fabricate biodegradable fibrous membranes with porous microstructures. Such fibrous membranes mimic the natural extracellular matrix structure for stem cells to migrate, adhere, proliferate, differentiate. In addition, flexible electrospun fibrous materials made by synthetic high-molecular-weight polymers or natural polymers or the blends of them can endow fiber materials with proper properties including mechanical property and regulatable biodegradation by changing the compositions and adjusting the blending ratios [9]. These membranes can also be easily cut into desired shapes to match tissue defects. Moreover, it is easy to incorporate bioactive agents into [10] fibers during electrospinning or onto the surface [11] of fibers to achieve sustained drug delivery. These features impart the electrospun fibrous membranes with translational promise.

Due to their low cost, high safety, biodegradability, and convenient availability, poly (ϵ -caprolactone) (PCL) and gelatin have been used as biomaterials for decades [12]. As their complementary characteristics in degradation speed and hydrophobicity, PCL and gelatin are frequently combined in blend electrospinning for biomedical applications [10, 13–15]. Nevertheless, osteogenic properties of PCL/gelatin membranes are often limited. To impart the electrospun membranes with tissue regeneration ability, bioactive growth factors (GFs), such as bone morphogenetic protein 2 (BMP-2) [16] and platelet-derived growth factor (PDGF) [17], were incorporated. However, the short protein half-life, possible denaturation as well as high cost have limited the use of bioactive GFs. Compared with bioactive GFs, nanomaterials with tissue regeneration ability possessed some unique advantages, such as high stability and relatively low cost. Therefore, numerous nanomaterials, such as bioactive glass nanoparticles [18], nano-hydroxyapatite (nHA) [19], gold nanoparticle (Au NP) [20], graphene oxide (GO) [21] and cerium oxide nanoparticles (CeO₂ NPs) [22], have been explored as bioactive agent substitutes for tissue engineering in bone defect healing [23]. Among them, CeO₂ NPs have a potential in improving healing process of different tissues which is attributed to their excellent biological properties including anti-oxidation, anti-inflammation, antibacterial activities and angiogenic potential [24]. Therefore, they have been applied in the therapy of drug-induced liver injury [25] and inflammatory bowel disease [26]. CeO₂ NPs have also been applied in bone tissue engineering because they can control the growth and differentiation of mesenchymal stem cells (MSCs) [27,28], promote bone regeneration on titanium surface [29] and enhance vascularization [30,31]. Interestingly, Ce exists in healthy bone and accumulates with ages [32]. However, the effects of CeO₂ NPs on periodontal ligament stem cells (PDLSCs, cells isolated and expanded from periodontal ligament tissue with “stemness”) [33] have not been explored yet.

In this work, to develop new membranous substitutes with a favorable ability on promoting bone regeneration for GTR and GBR application, we utilized electrospinning to prepare CeO₂ NPs loaded membranes. By taking advantage of the osteogenesis potential of CeO₂ NPs (as a bio-activator), the CeO₂ NPs loaded PCL/gelatin composite (PG-CeO₂) nanofibrous membranes were prepared. The effects of CeO₂ NPs on the osteogenic differentiation of hPDLSCs were first investigated. Furthermore, the PG-CeO₂ membranes were implanted into rat skull critical-sized bone defect models to evaluate their *in vivo* bone regeneration activity. It showed that CeO₂ NPs promoted proliferation and osteogenesis differentiation of hPDLSCs. When combined with electrospinning, PG-CeO₂ membranes exhibited promoted ability on bone regeneration, which implied they have potential application in alveolar bone regeneration for periodontal tissue engineering.

2. Experimental section

2.1. Materials

Poly (ϵ -caprolactone) (PCL, 80000 kD) and Gelatin (Gel, 300 g Bloom) were bought from Sigma-Aldrich. Hexafluoroisopropanol (HFP) were bought from Aladdin Reagent Company, acetic acid (HAc) were bought from Sinopharm. Cell Counting Kit-8 (CCK-8) were bought from Donjindo Molecular Technologies.

2.2. Synthesis of CeO₂ nanoparticles and fabrication of fibrous membranes

The CeO₂ NPs were synthesized according to a previous report [34] as the following process: cerium nitrate (6 mmol) was dissolved in 100 mL of H₂O and ethylene glycol solution (1:1) at room temperature. The cerium nitrate solution was heated up to 60 °C, and then 20 mL NH₄OH was introduced. CeO₂ NPs were obtained after vigorous stirring for 3 h. Then CeO₂ NPs were functionalized with carboxyl groups by citric acid treatment for better hydrophilicity. The fibrous membranes were fabricated by an electrospinning technique. PCL and Gelatin were dissolved in HFP, then HAc was added. The composition was listed in Table 1. After adding CeO₂ NPs, the solution was stirred and ultrasonically processed for 30 min. The electrospinning parameters were: voltage 16 kV, height 15 cm, flow rate 1 mL/h. The air humidity was 40%–60%. All the samples were collected on aluminum foil, and then lyophilized. After removal of the aluminum foil, the membranes were stored in clean polythene bags for the following experiments.

2.3. Characterization of the CeO₂ NPs and CeO₂ loaded fibrous membranes

X-ray powder diffraction (XRD) measurements of CeO₂ NPs were carried out in a D8-ADVANCE (Bruker AXS Inc, Madison, WI, USA). The size and distribution were studied by transmission electron microscopy (TEM, Tecnai G2 Spirit Biotwin, FEI Company, USA) and dynamic light scattering (DLS, Nano-ZS, Malvern Instrument). X-ray photoelectron spectroscopy (XPS) was performed using a PHI 5000 VersaProbe (Ulvac-Phi, Japan). Fibers with or without CeO₂ were observed by TEM as well. The fibers with or without CeO₂ NPs were coated by platinum and then the micromorphology was observed by scanning electron microscopy (SEM, S-3400 N II, Hitachi, Tokyo, Japan), equipped with a detector for energy dispersive spectroscopy (EDS). Those SEM images were used for fiber diameters measurement by the ImageJ software. Elemental analysis of cerium ions in fibrous membranes was conducted on an inductive coupled plasma optical emission spectrometer (ICP-OES, OPTIMA530DV, PerkinElmer). Mechanical properties detection was carried out at room temperature by using a universal testing machine (Instron 3365, USA). Samples were cut into rectangles (4 × 1 cm) and their thickness was measured by a micrometer caliper. The constant cross-head speed was set as 10 mm/min and stress-strain curves were recorded. Thermo-gravity analysis (TGA) was used to evaluate the variation of thermal stability of membranes in the presence or absence of CeO₂ NPs (TGA Simultaneous Thermal Analyzer, Mettler-Toledo, Switzerland). The *in vitro* degradation of fibers was detected by SEM for surface morphology change and degradation rates were calculated by weight loss in physiological solution on days 0, 1, 3, 7 and 14. Membrane samples were first weighted (W₀) and subsequently incubated in 5 mL PBS in EP tubes at 37 °C. Weights of every sample were

Table 1
The composition of electrospinning solution for membrane fabrication.

	HFP (mL)	PCL (g)	Gel (g)	HAc (μ L)	CeO ₂ NPs (g)
PCL/Gel	15	1.05	1.05	20	0
PCL/Gel/CeO ₂	15	1.05	1.05	20	0.105

recorded at predetermined time points (W_t) after drying. The remained mass rates were calculated as $W_t/W_0 \times 100\%$.

2.4. *In vitro* antioxidant study of CeO₂ NPs in membranes

The SOD-like activities of CeO₂ NPs in fibrous membranes were assessed by monitoring the change of $\bullet\text{O}_2^-$ by using nitro blue tetrazolium (NBT) as a probe [35]. Briefly, NBT (2 mM), EDTA (0.1 M) and riboflavin (1.2 mM) were mixed into Tris-HCl buffer (0.1 M, pH 7.4). After mixing for 5 min at 37 °C, PG-CeO₂ membranes (1 mg/mL) were added and irradiated with a LED lamp for 110 s. The absorption spectra of the mixed solution were then obtained by using a microplate reader. The CAT-like activities of CeO₂ NPs were assessed by measuring the amount of generated oxygen with a dissolved oxygen meter (SevenExcellence Multiparameter, Mettler Toledo Co., Ltd). After adding 3 mg PG-CeO₂ membrane into 3 mL H₂O₂ (0.5 M) solution, the amount of generated oxygen (mg/L) was detected and recorded every 30 s.

2.5. hPDLSCs culture and viability assay

Human PDL stem cells were obtained and identified as our previous work [36]. In short, premolars from young patients (aged < 16 y) were obtain from volunteers for orthodontic reasons with consent forms, and PDL tissue blocks were isolated from the middle third of the root surface and cultured in complete medium. Then, P0 cell suspension was seeded at the concentration of 500 cells/mL in 96-well plates for single cell-derived colonies selection. Those individual colonies were passaged and expanded for identification and following experiments. Cells of passage 3–5 were used. The cell viability and proliferation were detected by CCK-8. Briefly, the cells were cultured with CeO₂ NPs at different concentrations for 48 h. 10 μL of CCK-8 reagent was added into 100 μL medium each well for incubation, then the optical density (OD) was measured by a SpectraMax M3 microplate reader (Molecular Devices, CA, USA) at a wavelength of 450 nm every 30 min until the OD was 1.0–2.0. OD values of cell proliferation on days 1, 3, 5, and 7 were measured in the same way. For cell cycle detection, cells were stained by propidium iodide (PI, 50 $\mu\text{g}/\text{mL}$) which contained RNase (100 $\mu\text{g}/\text{mL}$), and then incubated for 30 min at 37 °C for flow cytometry (BD Biosciences, Mountain View, CA). The populations of the G1, G2 and S were quantified by the FlowJo software. Cells' debris and clumps were excluded.

2.6. TEM imaging of cells

To investigate intracellular CeO₂ localization, hPDLSCs were cultured with CeO₂ NPs for 24 h. Then the samples were washed by PBS for three times and fixed overnight in 2.5% glutaraldehyde. After that, the cells were post-fixed with 1% osmium tetroxide (Merck, Germany) for 2 h and dehydrated using graded ethanol series: 50, 75, 95 and 100% twice for 10 min and finally embedded in an epoxy resin for ultrathin sectioning. The sectioned samples were used for TEM imaging at an accelerating voltage of 120 kV.

2.7. Osteogenic differentiation

For cell osteogenic induction, the culture medium was changed by osteogenic differentiation medium (OS, growth medium supplemented with 0.1 μM dexamethasone, 10 mM β -glycerophosphate, and 50 μM ascorbic acid). Alkaline phosphatase (ALP) activity and Alizarin Red Staining (ARS) were performed to evaluate the osteogenic potential. ALP activity assay and NBT/BCIP ALP staining kits (Beyotime Biotechnology, China) were used to analyze the ALP activity according to the manufacturer's instructions on day 7. For ARS staining, 10% ARS solution (Sigma-Aldrich) was used to staining cells on day 21 for 5 min and washed by water. Then red mineral deposition that stained by ARS quantitation was applied by measuring the absorbance at 562 nm after

mineral nodes were desorbed by 10% (w/v) cetylpyridinium chloride (CPC, Sigma-Aldrich).

2.8. Real-time quantitative PCR

To evaluate the effect of CeO₂ NP on hPDLSCs' differentiation at different concentrations, *in vitro* co-culture of the cell and CeO₂ NP for 7 days was performed. Then, the expression of osteogenic-related genes was examined, including Runt-related transcription factor 2 (RUNX2), bone morphogenetic protein (BMP-2), osteocalcin (OCN), and osteopontin (OPN). All primer sequences were summarized in Table 2. Total cellular RNA was isolated by TRIzol (Invitrogen, Karlsruhe, Germany), then further reverse transcribed to cDNA using PrimeScript™ II 1st Strand cDNA Synthesis Kit for real-time polymerase chain reaction (RT-PCR, Takara, Japan). qRT-PCR was carried out using Universal SYBR Green Supermix (Bio-Rad, USA). Each reaction was performed in a final volume of 10 μL containing 1 μL cDNA, and 0.5 mM of each primer, 5 μL SYBR Green PCR Master Mix, and ddH₂O. The relative level of target gene expression was calculated using the comparative $2^{-\Delta\Delta\text{Ct}}$. All the samples were run in triplicate and normalized to GAPDH.

2.9. Western blot

Total cellular protein was extracted from cultured cell populations using the RIPA buffer (Thermo Scientific, Rockford, IL, USA) supplemented with protease inhibitor cocktail, following the manufacturer's specifications. Protein concentration was measured by the Bradford method (Bio-Rad Laboratories, Benicia, CA, USA) with bovine serum albumin (BSA) as a standard. Protein samples were loaded at 10 μg protein per well on 4%–20% sodium dodecyl sulfate (SDS)-polyacrylamide gel electrophoresis (SDS-PAGE) and transferred to polyacrylamide fluoride (PVDF) membranes. The membranes were blocked with 3% BSA in PBST (PBS with 0.1% Tween). Primary antibodies of ALP, BMP-2, OPN, and OCN (Abcam, Cambridge, MA, USA) were applied in 1:500 dilution. Immune complexes were detected with anti-rabbit secondary antibody (Abcam, Cambridge, MA, USA) and chemiluminescence reagents. The amount of protein expression was compared after normalization with β -actin.

2.10. Cell morphology on fibrous membranes

Fibrous membranes with CeO₂ NPs were immersed in 75% ethanol for 20 min in sterile culture dishes, then washed in ddH₂O for three times, rinsed from PBS with 10% penicillin/streptomycin 3 times, and soaked in DMEM overnight before cell seeding. Cells cultured on the membranes for 1, 3, 5, and 7 days. The samples were washed thrice with PBS and fixed with 2.5% glutaraldehyde overnight at 4 °C. Next, those samples were progressively dehydrated with 10%, 20%, 30%, 40%, 50%, 60%, 70%, 80%, 90% and absolute ethanol for 10 min, respectively. Then the samples were air-dried for SEM observation of cell morphology.

2.11. In vivo experimental design

The membranes were cut into discs with a diameter of 5 mm. The sterilization of samples was performed with UV-light irradiation and

Table 2
Primer sequences.

Gene	Forward primer sequence (5'–3')	Reverse primer sequence (5'–3')
RUNX2	GGAGTGGACGAGGCAAGAGTTT	AGCTTCTGTCTGTGCCTTCTGG
BMP-2	TAGTGACTTTTGGCCACGACG	GCTTCCCGCTGTTTGTGTTTG
OCN	GGCAGCGAGGTAGTGAAGAG	GATGTGGTCAGCCAACCTCGT
OPN	GATGGCCTTGTATGCACCATTG	GCAGACCTGACATCCAGTACC
GAPDH	CGCTCTCTGCTCCTCTGTT	CCATGGTGTCTGAGCGATGT

75% ethanol treatment, then washed and immersed by DMEM with 10% penicillin/streptomycin for 24–48 h. The rat cranial defect model was used to evaluate bone regeneration in this study. Thirty Sprague-Dawley rats (male, 7–8 weeks old) were divided into three groups: control group (defects without repair), PG membrane group, and PG-CeO₂ membrane group. After anesthetized by pentobarbital sodium, the rats were positioned in a stereotaxic frame and immobilized during surgery. The hairs over the skull were shaved, then a surgical incision along the midline from the nasofrontal to the occipital region was made for dorsal calvarium exposure. A saline-cooled stainless-steel trephine (5 mm outer diameter) was used to remove full-thickness bones to create defects on both left and right sides of the dorsal calvarium for membrane implantation. After the implantation for 4 weeks and 8 weeks, 5 rats in each group were sacrificed, and their calvarias were collected and fixed in 10% neutral buffered formalin for Micro-CT (VivaCT 80, Scanco Medical, Switzerland) analysis. The parameters for scanning were set as source voltage at 70 kV, source current at 114 μ A and the scanning slice thickness was 18 μ m. Then decalcified for histological evaluation. Three-dimensional (3D) pictures and bone volume (BV)/tissue volume (TV) ratios were reconstructed and analyzed. After that, those samples were decalcified in EDTA-Na₂, then embedded in paraffin for sectioning. Haematoxylin-eosin (HE) and Masson's trichrome staining were performed.

2.12. Data analysis

Data were expressed as the mean \pm standard deviation (SD). At least three duplicate samples were tested in all experiments.

2.13. Ethics approval and consent to participate

The animal experiments were carried out with the approval of the

Ethics Committee and guidelines of the Animal Care Committee of Nanjing Medical University (IACUC-1912027). Teeth were taken after informed consent of the patients. The manuscript does not contain clinical studies or patient data.

3. Results

3.1. Characterization of CeO₂ NPs and cell biocompatibility evaluation

As prepared CeO₂ NPs aqueous solution (Fig. 1a) appeared as an orange colloidal solution with evenly dispersible CeO₂ NPs, XRD pattern of CeO₂ NP sample (Fig. 1b) showed diffraction peaks matched the standard diffraction pattern of CeO₂ NPs without impure peaks, confirming the single cubic phase of crystalline CeO₂ NPs. As shown in TEM (Fig. 1c) and DLS (Fig. 1d) images, CeO₂ NPs were well dispersed, and their average particle size was 8.1 ± 4.6 nm. The long-term stability of CeO₂ NPs was investigated by DLS. After storing for more than 6 months, CeO₂ NPs are still well dispersed in water, demonstrating that the long-term stability of CeO₂ NPs was quite good (Fig. S1). Since the ratio of Ce³⁺ to Ce⁴⁺ on their surfaces is an important property of CeO₂ NPs, XPS spectrum was collected to quantify the ratio of the Ce species. As shown in Fig. S2, both the Ce³⁺ and Ce⁴⁺ existed on CeO₂ NPs' surface, and the Ce³⁺ fraction was 29.87%. As shown in Fig. 1e–f, concentrations of CeO₂ NPs up to 100 μ g/mL had no significant effect on cell viability. CeO₂ NPs seemed to promote cell proliferation when co-cultured for more than 3 days. And also, after incubating CeO₂ NPs with hPDLSCs for 48 h, cells had little morphological change (Fig. 1g), and negligible cell cycle change (Fig. 1h–i), more than 90% of cells were at the G1 phase. These results indicated that the CeO₂ NPs had good biocompatibility. Based on the above results, we chose four concentrations of CeO₂ NPs (0, 10, 50, and 100 μ g/mL) to investigate the effects of CeO₂ NPs on the osteogenic differentiation of hPDLSCs.

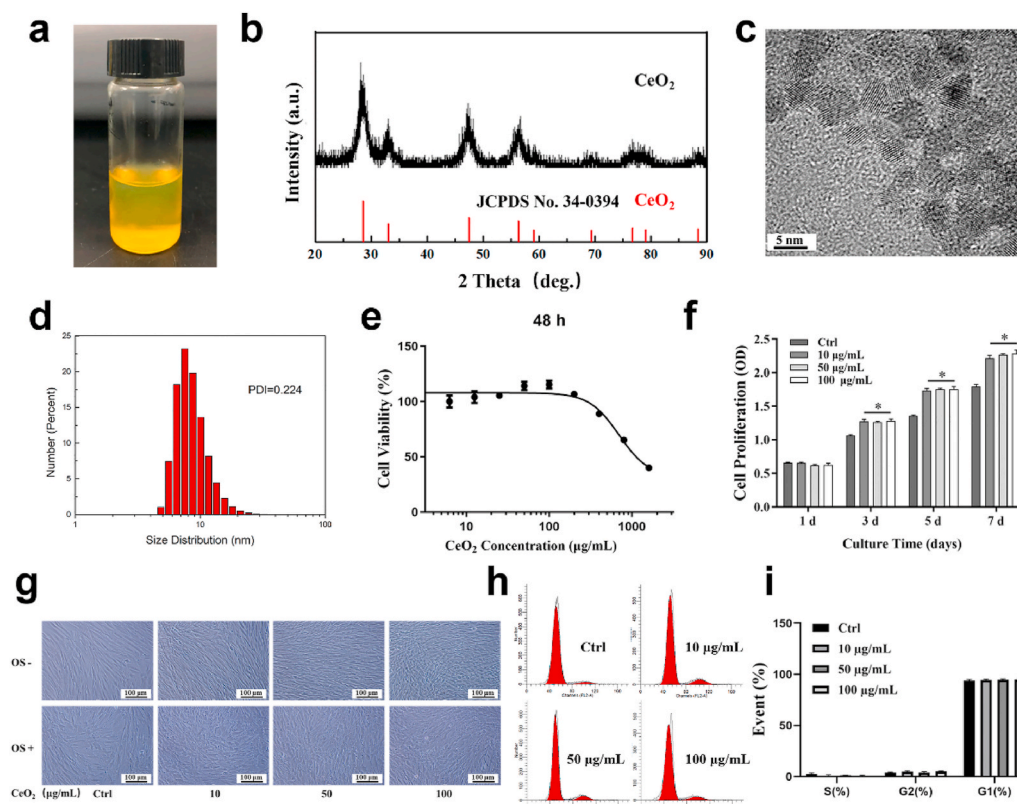


Fig. 1. Characterization and biocompatibility of CeO₂ NPs. (a) Digital photo, (b) XRD pattern, (c) TEM image and (d) size distribution histogram of CeO₂ NPs. (e) Viability and (f) proliferation of hPDLSCs when treated with CeO₂ NPs at different concentrations. (g) Light microscope images of hPDLSCs when culture with or without CeO₂ NPs under normal (OS-) and osteogenic induction medium (OS+). (h, i) Cell cycle analysis of hPDLSCs treated with CeO₂ NPs for 3 days.

3.2. Internalization and localization of CeO₂ NPs in hPDLSCs

Ultrastructural analysis was performed to detect the localization of CeO₂ NPs within the cells. Typical TEM images (Fig. 2) of cells after incubation with 10 µg/mL CeO₂ NPs for 24 h showed that the cells incubated with CeO₂ NPs contain black dots corresponding to clusters of aggregated particles, whereas these dots were not observed in the cells incubated without NPs. CeO₂ NPs were uptake by hPDLSCs, and endosomal compartments containing nanoparticles were seen inside the cells.

3.3. In vitro effects of CeO₂ NPs on osteogenic differentiation

The impact of CeO₂ NPs on osteogenic differentiation of hPDLSCs was evaluated by ALP activity and staining, RT-PCR, and Western Blot. hPDLSCs were cultured with CeO₂ NPs in OS medium. ALP activity was tested by ALP activity assay and ALP staining. On day 7, ALP activity levels of hPDLSCs were increased when incubating with CeO₂ NPs at different concentrations (Fig. 3a). The effects of CeO₂ NPs on the formation of the mineralized nodules were tested by ARS on day 21, by which calcium nodule can be stained red, and histogram image of CPC quantification on the left (Fig. 3b). The gene expressions of bone-related mRNA (RUNX2, BMP-2, OCN and OPN) (Fig. 3c), and protein expression levels (ALP, BMP-2, OCN and OPN) (Fig. 3d) were also detected. Those results had a consistent trend in our study, in which the osteogenic markers of hPDLSCs were all up-regulated at all concentrations of CeO₂ NPs, while with no statistical significance. Taken together, these results showed that CeO₂ NPs significantly promoted hPDLSCs osteogenic differentiation even at the lowest concentration of 10 µg/mL.

3.4. Characterization of fibrous membranes incorporated with CeO₂ NPs

For utilizing CeO₂ NPs in periodontal regeneration in a proper way, electrospinning was selected for the NPs encapsulation and local delivery. Fig. 4a showed the process of electrospinning to fabricate membranes. When the original fiber jet was stable, it was swapped to the fiber formation mode and the samples were collected as non-woven membranes. TEM and SEM images of fibers without or with CeO₂ NPs were presented in Fig. 4b and d, 4c and 4e, respectively. The fiber with CeO₂ NPs had black particles inside, indicating the successful encapsulation of CeO₂ NPs (Fig. 4c). SEM images showed both kinds of fibers were macroscopically smooth without any gross defects. The average diameter of blank fibers and fibers with CeO₂ was 378 ± 204 nm and 355 ± 181 nm, respectively. There was no statistical significance between the two types of fibers. To confirm CeO₂ NPs were incorporated in fibrous membranes, EDS mapping was presented in Fig. 4f–h, which showed Ce, O, and C elements were in the fiber, and the atomic percent of Ce was 3.8%. And also, the result of inductive coupled plasma optical emission spectrometer (ICP) showed weight ratio of Ce in the composite was 3.84%, which means the proportion of CeO₂ was 4.72%. Those results demonstrated CeO₂ NPs have been successfully incorporated

inside the fibers.

Fig. 5a–c showed the mechanical properties of membranes, the ultimate tensile strength data of PG and PG-CeO₂ were 2.15 ± 0.32 MPa and 5.46 ± 0.40 MPa. The stress at failure data were 25.6 ± 6.02 and 77.09 ± 9.71, and the data of Young's modulus were 44.00 ± 3.00 MPa and 60.64 ± 8.67 MPa, respectively. All three parameters showed the mechanical properties of membrane with CeO₂ NPs were remarkably enhanced. In addition, the representative tensile stress-strain curves of membranes were showed in Fig. 5d, indicating that both of the membranes were elastic. TGA technique was used to evaluate the thermal stability of membranes. As shown in Fig. 5e, the initial degradation temperature of PG-CeO₂ membrane was slightly lower than PG membrane, but the mass loss had a consistent trend because the main composite of both membranes was PCL and gelatin. Membranes degraded gradually in physiological solution, which was recorded by weight measurements and SEM. As shown in Fig. 5f, there was a sharp drop of weight in the first week of both groups. Compared with PG membrane, the weight loss was more prominent in PG-CeO₂ membrane group, which may be attributed to the incorporation of CeO₂ NPs. While at the second week, weight loss slowed down. The reason may be attributed to the release of CeO₂ NPs that speed up the degradation of fibers by providing an increase in surface area of fibers at the first week. The same trend was observed in SEM images. Fibers had significant morphological changes during the immersion, and fibers became rough and fused. Compared with the PG membrane, micropore appeared in fibers of PG-CeO₂ membranes on day 7 and became more obvious on day 14, which might be attributed to the CeO₂ release from fibers. To further verify it, EDS mappings of PG-CeO₂ membranes on days 3, 7 and 14 in the degradation test were collected as well. As shown in Fig. S3, the atomic ratio of Ce was decreasing along with the extension of soak time in PBS, from 3.8% before immersion, to 0.6%, 0.5% and 0.3% on days 3, 7 and 14, respectively. Those results verified incorporation of CeO₂ can affect degradable speed and fiber morphology to a certain extent, and also proved the release of CeO₂ from membrane along with degradation.

To investigate whether the process of electrospinning affects the ROS-scavenging activity of CeO₂ NPs, *in vitro* antioxidant capacity of CeO₂ NPs that incorporated in membranes had been examined. As shown in Fig. S4, ROS can be eliminated by adding PG-CeO₂ membranes, which proved CeO₂ NPs in electrospun membranes still have SOD-like (Fig. S4a) and catalase-like (Fig. S4b) activities.

3.5. Cell behavior of hPDLSCs co-culture with membranes

The morphology and distribution of hPDLSCs onto PG-CeO₂ membranes after culturing for 1, 3, 5, and 7 days (Fig. 6a), and partial enlarged SEM images were presented in Fig. 6b. The results demonstrated that cells were captured by fibers after co-cultured for 1 day. Then with the extending of culture time, cells spread out on the surface and infiltrated inside gradually. A week later, the surface of the membrane was almost covered by hPDLSCs. We also detected cell

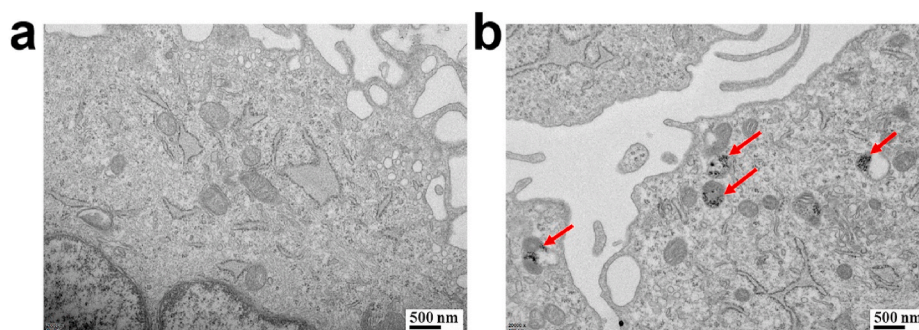


Fig. 2. (a) TEM image of hPDLSCs. (b) hPDLSCs treated with CeO₂ NPs for 24 h (red arrows: CeO₂ NPs). (For interpretation of the references to colour in this figure legend, the reader is referred to the Web version of this article.)

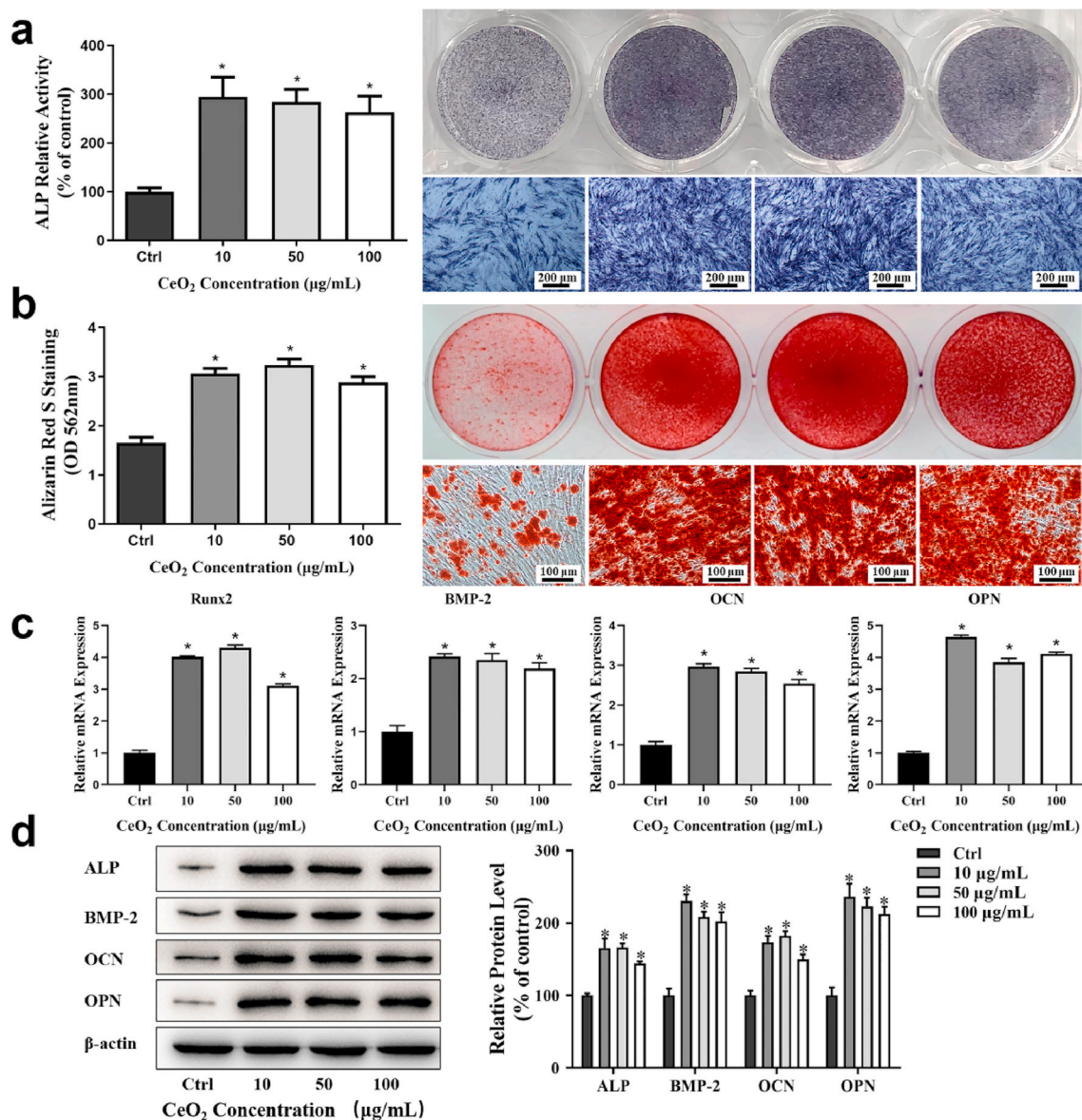


Fig. 3. Osteogenic effects of CeO₂ NPs on hPDLSCs after co-cultured at concentration of 0, 10, 50, and 100 μg/mL (a) ALP relative activity (left) and corresponding stained images (right) on day 7. (b) ARS assay of mineralization, OD values at 562 nm (left) and corresponding stained images (right) on day 21. (c) Osteogenic related gene expressions on day 7. (d) Osteogenic related protein expressions on day 14.

proliferation on membranes. Cells seeded on PG-CeO₂ membranes obviously promoted cell growth in comparison with blank PG membranes on day 7 (Fig. 6c), while without significant statistical significance on the previous days (day 1, 3, and 5). And the ALP activity of hPDLSCs was increased when cultured with blank PG membranes, and further improved by the addition of CeO₂ NPs (Fig. 6d).

3.6. Micro-CT analysis

The surgical procedures of materials implantation were presented in Fig. 7a. After 4 weeks and 8 weeks' implantation, the samples of animal calvaria were extracted and assessed by Micro-CT. At the time point of 4 weeks, limited new bone regeneration was observed in the control group (Fig. 7b). In contrast, PG membranes can provide mechanical and space support for cell growth, proliferation and differentiation, and CeO₂ NPs can promote the regenerative process. As time went to 8 weeks, each group had more new bone regenerated, the defect area was almost reconstructed in the group of PG-CeO₂ membrane. These results were further quantitatively analyzed by calculating the BV/TV (Fig. 7c),

which were consistent with the Micro-CT results. The PG-CeO₂ membrane group had the highest BV/TV ratio and had significantly statistical differences at week 8.

3.7. Histological section results

HE and Masson staining of histological sections were shown in Fig. 8. When implanted *in vivo* for 4 weeks, in the control group (Fig. 8a, d, g, j), there was only connective tissue regenerated with little bone formation, while in implant groups (PG M and PG-CeO₂ M), new bone restored the defect along the fibrous membranes. The maximum amount of bone regenerated was the PG-CeO₂ membrane group (Fig. 8c, f, i, l), better than the PG membrane group (Fig. 8b, e, h, k), reflected in much more mature and thicker new-formed bone in both 4 weeks and 8 weeks. Because the Masson staining images can clearly distinguish bone and fibrous tissues clearly, microphotographs of Masson staining were locally enlarged (Fig. 9) to further analyze the structure of defect parts. In the control group of both 4 weeks and 8 weeks, defects were filled with fibrous tissue and very limited nascent bone was observed. In the

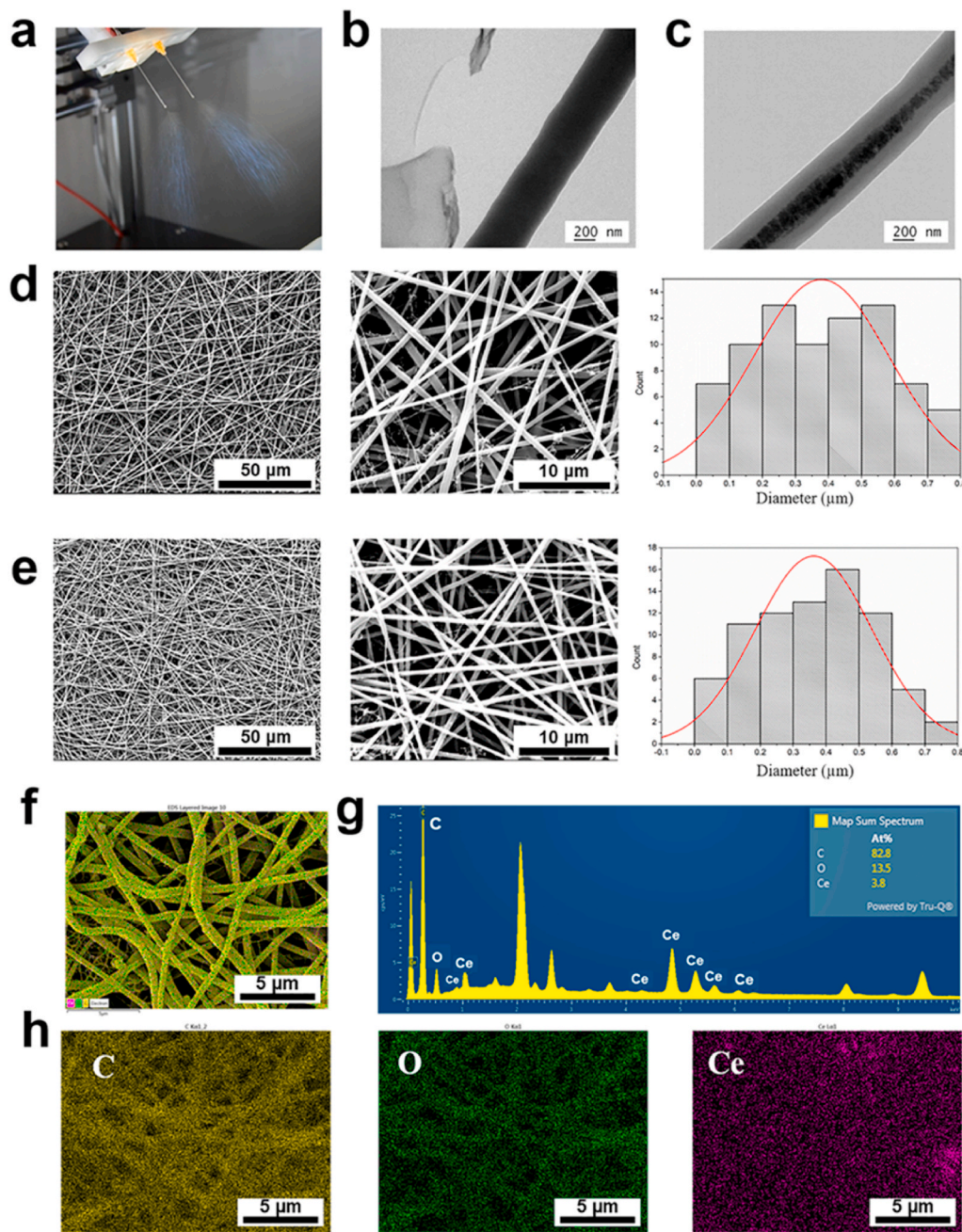


Fig. 4. (a) Photograph of electrospinning. Representative TEM images of (b) PG fiber and (c) PG-CeO₂ fiber. Representative SEM images with histograms of fiber diameters of PG membranes (d) and PG-CeO₂ fibrous membranes (e). EDS elemental mapping for the merged image of all elements (f), spectrum (g) and elements C in yellow, O in green, Ce in purple (h). (For interpretation of the references to colour in this figure legend, the reader is referred to the Web version of this article.)

PG membrane group, new bone was formed on the surface of membrane at week 4 (Fig. 9b), and the bone mass became thicker at week 8 (Fig. 9e). In the PG-CeO₂ membrane group, consistent with PG membrane group, nascent bone was formed along the membrane at week 4 (Fig. 9c), and accumulated to almost fully fill the defect at week 8 (Fig. 9f).

4. Discussion

As is well known, in the therapy of oral diseases, bone regeneration is quite essential for the reconstruction of teeth supporting tissue and providing space for dental implants. Many strategies [37,38] about promoting the osteogenic differentiation of stem cells toward enhanced bone regeneration have been carried out in recent years, such as the

usage of NPs [20,39] and the modification of bone tissue engineering scaffolds [40–42]. Here, we introduced CeO₂ NPs that are promising materials in various biological applications [43] as a bioactive factor to promote bone regeneration, a crucial part of periodontal tissue regeneration. We further combined CeO₂ NPs with electrospun membranes for repairing rat cranial defects *in vivo*.

Cell biocompatibility of nanomaterials was a requirement in their potential biological application [44]. Our results shown in Fig. 1 indicated that CeO₂ NPs had good biocompatibility, and even up-regulated cell proliferation at low concentrations, which was consistent with the effects on the BMSCs viability [29] and primary mouse embryonic fibroblasts proliferation [45]. Stem cells are usually sensitive to the cellular uptake of NPs, because the NPs inside the cytoplasm might disturb cell fate and their ability in tissue regeneration [46]. In our

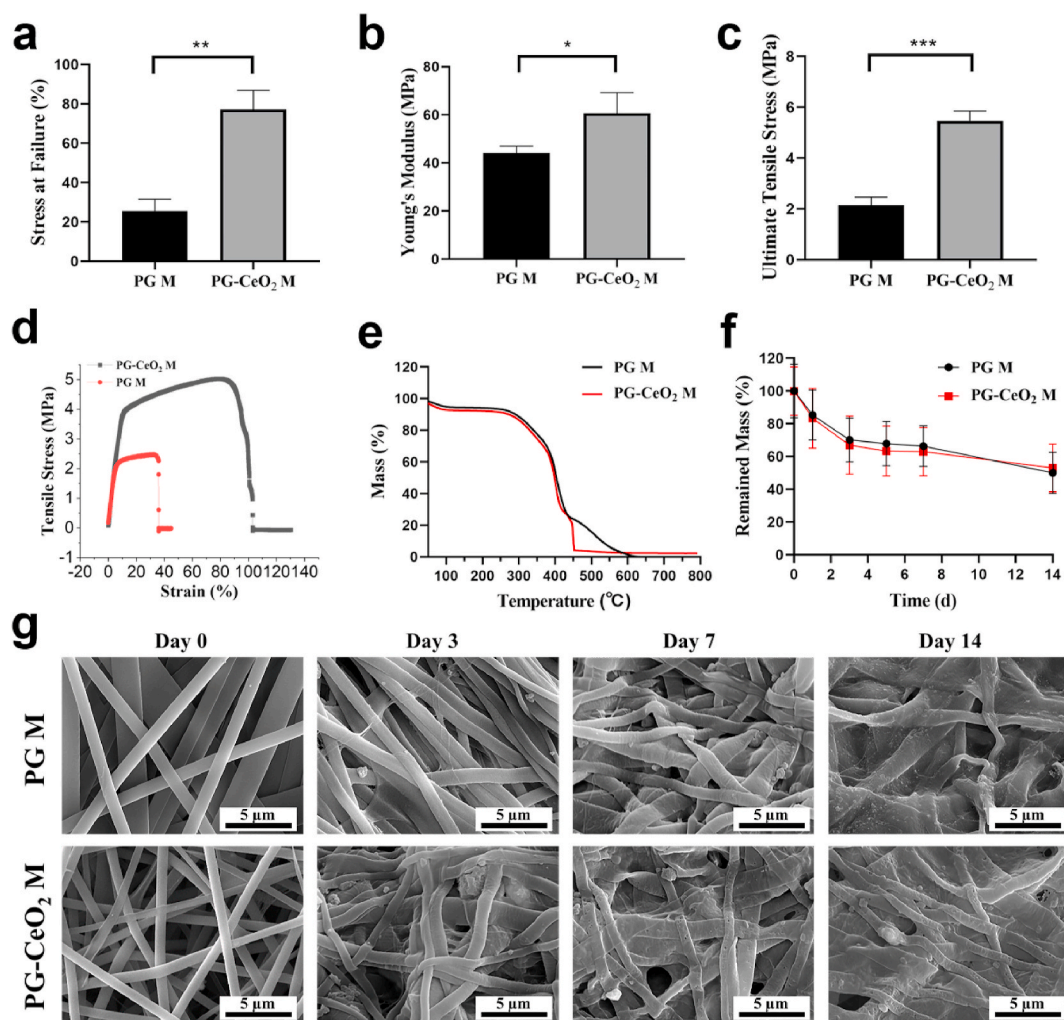


Fig. 5. (a) Strain at failure, (b) Young's modulus, (c) ultimate tensile stress ($n = 3$), and (d) representative tensile stress-strain curves of membranes. (e) TGA curves. (f) Degradation profiles and (g) SEM images of fibers on days 0, 3, 7, and 14 during the degradation in PBS.

study, CeO₂ NPs were up-taken by hPDLSCs and located inside vesicular membrane (Fig. 2b). Compared with blank hPDLSCs shown in Fig. 2a, CeO₂ NPs did not provoke apparent cell structural damage. However, this result was inconsistent with a previous study showing that CeO₂ NPs aggregated and retained inside the cytoplasm of cardiac progenitor cells [47]. The difference could be due to the particle size and incubation time of NPs with cells. As we know, the senescence of *in vitro* culture over passing and inflammation stimuli of stem cells lead to the ascent of ROS levels and oxidative injury [48]. Interestingly, intracellular CeO₂ NPs might protect stem cells' physiological function from such oxidative injury by scavenging excessive ROS and thus reducing the ROS-related damage of intracellular components including DNA fragmentation, lipid rupture and protein degradation [49]. This could be a well explanation of the observed good cellular biocompatibility of CeO₂ NPs.

Moreover, interactions between nanomaterials and stem cells affect the self-renewal and differentiation behaviors of stem cells [50,51]. To our delight, the CeO₂ NPs enhanced osteogenic differentiation-associated markers of hPDLSCs, such as ALP activity at the early stage and mineralized nodules at the later stage (Fig. 3). This is consistent with the previous studies that CeO₂ NPs could promote proliferation of stem cells, and played a positive role in new bone regeneration when combined with mesoporous bio-glass scaffolds [52] and gelatin-alginate scaffolds [53]. Ceria nanoparticles have been reported to promote hypertrophic differentiation of BMSCs via DHX15 activation on bone regeneration enhancement [54]. Nevertheless, it should be

noted that more work is needed to explore how the CeO₂ NPs promote osteogenic differentiation of hPDLSCs in the future.

Electrospinning was used as a fibrous membrane preparation technology to load CeO₂ NPs for evaluation of *in vivo* osteogenic effect. Biodegradable PCL and gelatin were utilized as a matrix to fabricate PG-CeO₂ electrospun membranes (Fig. 4c). PCL has suitable tensile property and biocompatibility, and it has been approved for biomedical applications by the U.S. Food and Drug Administration (FDA). However, PCL is hydrophobic and lacks bioactive sites for cell adhesion. Gelatin was therefore used to blend to enhance cell capture on scaffolds by increasing hydrophilicity [10,55]. The characterization of fibrous membranes incorporated with CeO₂ NPs (Figs. 4 and 5), which is important for further regenerative studies. As CeO₂ NPs used in our work were small, there was no obvious morphological change of fibers loaded with NPs, while the mechanical properties had been improved in PG-CeO₂, as well as in PLLA/gelatin composite membrane doped with CeNP [56] and MgO [57]. The anti-oxidative activities of CeO₂ are essential in its biomedical application. In this work, CeO₂ NPs that were loaded in the electrospun membrane have ROS-scavenging activity (Fig. S4), which also had been proved in a previous study [58].

Fig. 6a and b showed that hPDLSCs were captured, adhered and proliferated on the PG-CeO₂ membranes. Compared with cells seeded on blank PG membranes, cells on PG-CeO₂ membranes had a faster proliferation rate (Fig. 6c) on day 7. The enhanced proliferation was probably because of the degradation of gelatin induced release of CeO₂ NPs,

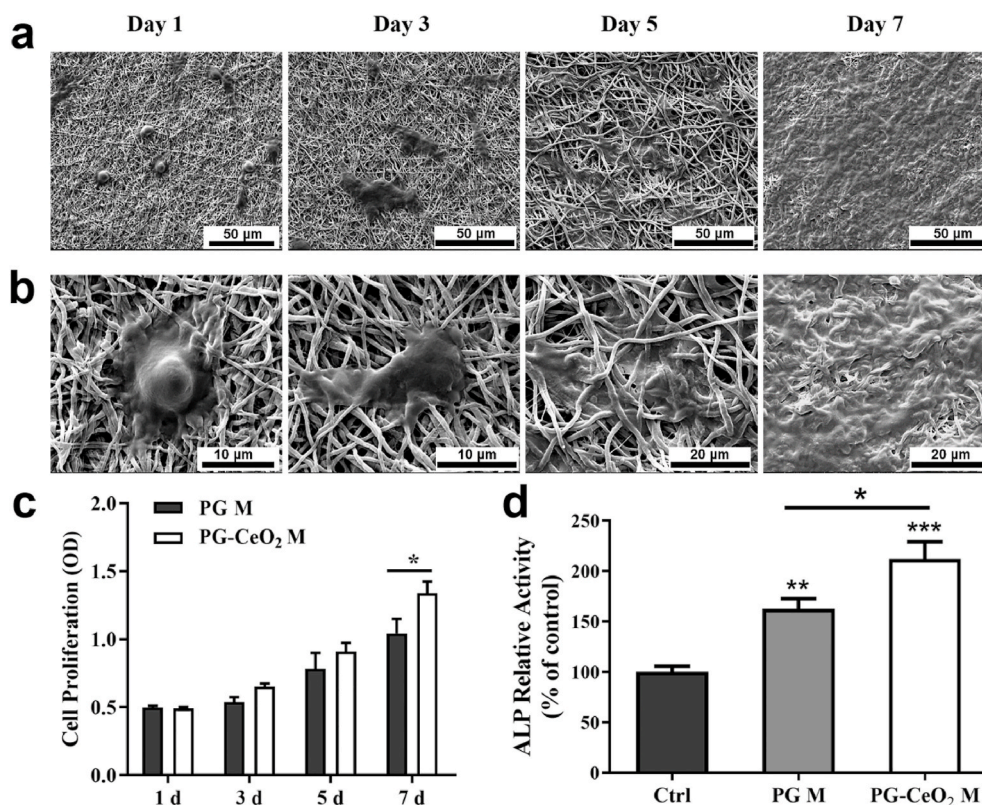


Fig. 6. Representative SEM images of cells on the membranes after seeded for 1, 3, 5, and 7 days (a and b). The images show the adherence and morphology of the cells. (c) Cell proliferation on the membranes after seeded for 1, 3, 5, and 7 days. (d) ALP activity of hPDLSCs on membranes on day 7. (n = 3), * $P < 0.05$, ** $P < 0.01$, *** $P < 0.001$.

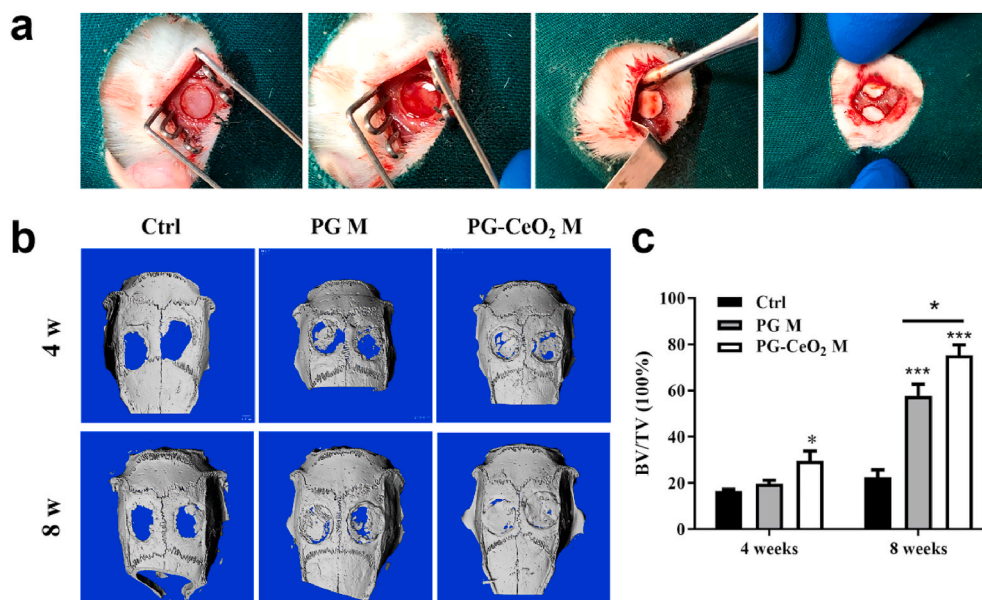


Fig. 7. (a) Photographs of the surgical procedure during membranes implantation. (b) Micro-CT evaluation and (c) quantitative analysis of bone growth within harvested samples. BV/TV: ratio of bone volume and tissue volume bone. (n = 5), * $P < 0.05$, ** $P < 0.01$, *** $P < 0.001$.

which promoted cell proliferation as the same trend in Fig. 1f. ALP activity shown in Fig. 6d, in agreement with Fig. 3a about the effect of CeO₂ NPs and a previous study [13] about non-woven PG membranes, demonstrates that PG-CeO₂ membranes could be used as a potential bone tissue engineering scaffold on promoting osteogenic differentiation of stem cells.

In our *in vivo* study of animal models of critical-sized cranial defect, the rate and quality of new bone formation agreed with the above *in vitro* results (Fig. 7b and c). The implantation of membranes could provide mechanical support for stem cells facilitating cell migration to the central part of the defect (Figs. 8 and 9). On the other hand, biophysical signals of biomaterials and force application had proved important in

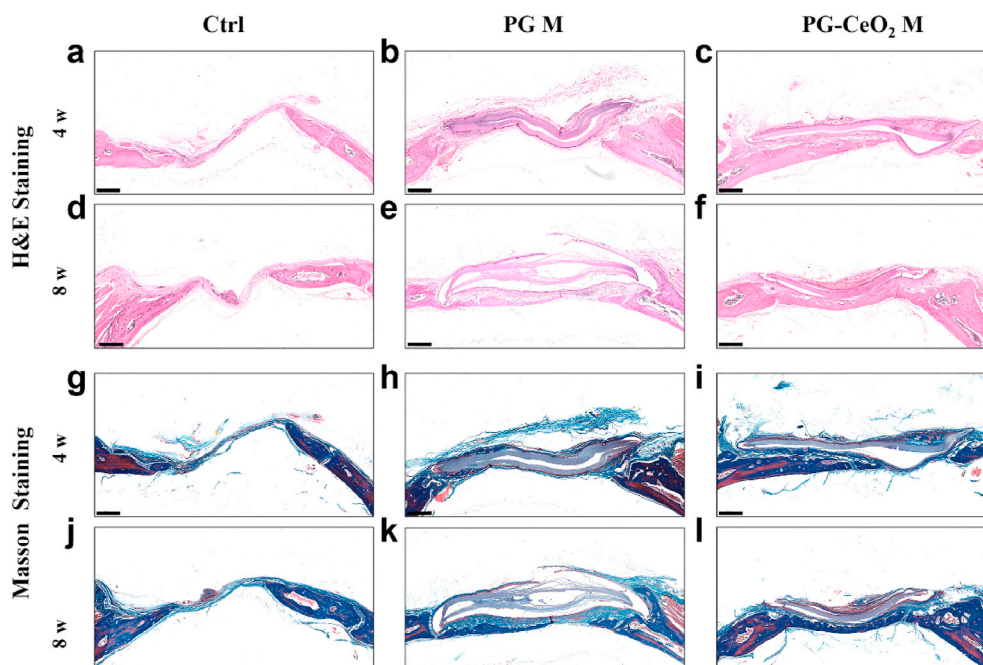


Fig. 8. HE and Masson's trichrome staining of rat cranial defects after implanted with PCL/gelatin membranes without or with CeO₂ NPs for 4 weeks and 8 weeks. Scale bars: 500 μ m.

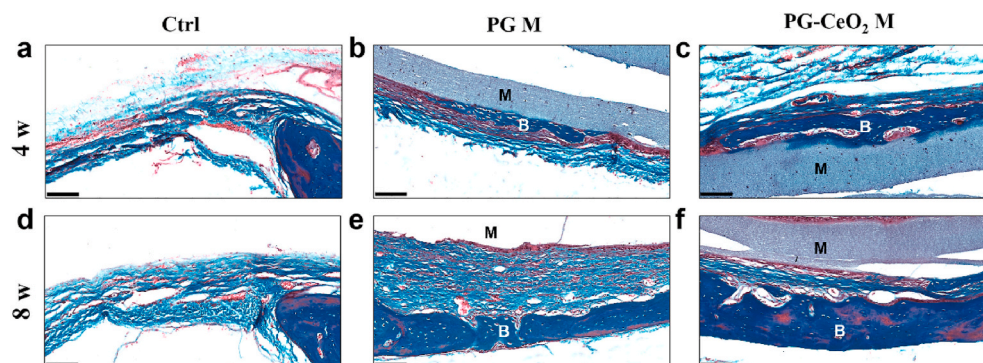


Fig. 9. Masson's trichrome staining of rat cranial defects at higher magnification. M: membrane, B: bone. Scale bars: 100 μ m.

stem cell fate regulation [59], stem cell fate can be influenced by cell geometry through plasma membrane order modulation [60], disordered structure of fibers with an arbitrary angle direction might stimulate osteo-differentiation of hPDLSCs [36]. CeO₂ NPs further increased the osteogenic differentiation ability of stem cells that homing to the membrane that implanted in defect parts.

5. Conclusions

In summary, we explored the effects of CeO₂ NPs on the behavior and function of hPDLSCs. The *in vitro* data proved that CeO₂ NPs promoted hPDLSCs osteogenesis differentiation. The *in vivo* study demonstrated PG-CeO₂ membranes accelerated bone regeneration comparing with blank PG membranes, which further certified the possible roles of CeO₂ NPs in new bone formation. We believe CeO₂ NPs have great potential in the treatment of periodontal disease and electrospinning could be a suitable way to integrate CeO₂ NPs and other nanomaterials in GTR/GBR for convenient clinical practices.

Declaration of competing interest

The authors declare that they have no competing interests.

CRediT authorship contribution statement

Shuangshuang Ren: Conceptualization, Data curation, Investigation, Methodology, Writing – original draft, Funding acquisition. **Yi Zhou:** Investigation, Methodology, Formal analysis, Writing – original draft. **Kai Zheng:** Investigation, Data curation, Writing – original draft. **Xuanwen Xu:** Validation, Data curation. **Jie Yang:** Validation, Data curation. **Xiaoyu Wang:** Validation, Formal analysis, Data curation, Writing – original draft. **Leiyang Miao:** Conceptualization, Project administration. **Hui Wei:** Conceptualization, Project administration, Writing – review & editing, Supervision. **Yan Xu:** Conceptualization, Funding acquisition, Project administration, Writing – review & editing, Supervision.

Acknowledgments

This work was supported by the National Natural Science Foundation

of China (No. 82001049, 81771074), the Priority Academic Program Development of Jiangsu Higher Education Institutions (PAPD, 2018–87), the Natural Science Foundation of Jiangsu Province (BK. 20200665). The authors are grateful to Professor Yong Hu (Nanjing University) for his critical support on electrospinning technology and valuable discussion of the project.

Appendix A. Supplementary data

Supplementary data to this article can be found online at <https://doi.org/10.1016/j.bioactmat.2021.05.037>.

References

- G. Hajishengallis, Periodontitis: from microbial immune subversion to systemic inflammation, *Nat. Rev. Immunol.* 15 (1) (2015) 30–44.
- D.F. Kinane, P.G. Stathopoulou, P.N. Papapanou, Periodontal diseases, *Nat. Rev. Dis. Primers* 3 (2017), 17038.
- S.S. Dominy, C. Lynch, F. Ermini, M. Benedyk, A. Marczyk, A. Konradi, M. Nguyen, U. Haditsch, D. Raha, C. Griffin, L.J. Holsinger, S. Arastu-Kapur, S. Kaba, A. Lee, M. I. Ryder, B. Potempa, P. Mydel, A. Hellvard, K. Adamowicz, H. Hasturk, G. D. Walker, E.C. Reynolds, R.L.M. Faull, M.A. Curtis, M. Dragunow, J. Potempa, *Porphyromonas gingivalis* in Alzheimer's disease brains: evidence for disease causation and treatment with small-molecule inhibitors, *Sci. Adv.* 5 (1) (2019) eaau3333.
- C.C. Villar, D.L. Cochran, Regeneration of periodontal tissues: guided tissue regeneration, *Dent. Clin. North. Am.* 54 (1) (2010) 73–92.
- M.C. Bottino, V. Thomas, G. Schmidt, Y.K. Vohra, T.M. Chu, M.J. Kowolik, G. M. Janowski, Recent advances in the development of GTR/GBR membranes for periodontal regeneration—a materials perspective, *Dent. Mater.* 28 (7) (2012) 703–721.
- Y. Liang, X. Luan, X. Liu, Recent advances in periodontal regeneration: a biomaterial perspective, *Bioact. Mater.* 5 (2) (2020) 297–308.
- J. Fang, R. Liu, S. Chen, Q. Liu, H. Cai, Y. Lin, Z. Chen, Z. Chen, Tuning the immune reaction to manipulate the cell-mediated degradation of a collagen barrier membrane, *Acta Biomater.* 109 (2020) 95–108.
- Y. Qian, X. Zhou, F. Zhang, T.G.H. Diekwisch, X. Luan, J. Yang, Triple PLGA/PCL scaffold modification including silver impregnation, collagen coating, and electrospinning significantly improve biocompatibility, antimicrobial, and osteogenic properties for orofacial tissue regeneration, *ACS Appl. Mater. Interfaces* 11 (41) (2019) 37381–37396.
- J. Xue, T. Wu, Y. Dai, Y. Xia, Electrospinning and electrospun nanofibers: methods, materials, and applications, *Chem. Rev.* 119 (8) (2019) 5298–5415.
- Y. Wang, W. Cui, X. Zhao, S. Wen, Y. Sun, J. Han, H. Zhang, Bone remodeling-inspired dual delivery electrospun nanofibers for promoting bone regeneration, *Nanoscale* 11 (1) (2018) 60–71.
- Y. Hu, W. Dan, S. Xiong, Y. Kang, A. Dhinakar, J. Wu, Z. Gu, Development of collagen/polydopamine complexed matrix as mechanically enhanced and highly biocompatible semi-natural tissue engineering scaffold, *Acta Biomater.* 47 (2017) 135–148.
- E. Malikmammadov, T.E. Tanir, A. Kiziltay, V. Hasirci, N. Hasirci, PCL and PCL-based materials in biomedical applications, *J. Biomater. Sci. Polym. Ed.* 29 (7–9) (2018) 863–893.
- M. Gong, C. Chi, J. Ye, M. Liao, W. Xie, C. Wu, R. Shi, L. Zhang, Icarin-loaded electrospun PCL/gelatin nanofiber membrane as potential artificial periosteum, *Colloids Surf. B* 170 (2018) 201–209.
- J. Xue, M. He, H. Liu, Y. Niu, A. Crawford, P.D. Coates, D. Chen, R. Shi, L. Zhang, Drug loaded homogeneous electrospun PCL/gelatin hybrid nanofiber structures for anti-infective tissue regeneration membranes, *Biomaterials* 35 (34) (2014) 9395–9405.
- R. Shi, H. Geng, M. Gong, J. Ye, C. Wu, X. Hu, L. Zhang, Long-acting and broad-spectrum antimicrobial electrospun poly (ϵ -caprolactone)/gelatin micro/nanofibers for wound dressing, *J. Colloid Interface Sci.* 509 (2018) 275–284.
- Y.J. Seong, E.H. Song, C. Park, H. Lee, I.G. Kang, H.E. Kim, S.H. Jeong, Porous calcium phosphate-collagen composite microspheres for effective growth factor delivery and bone tissue regeneration, *Mater. Sci. Eng. C Mater. Biol. Appl.* 109 (2020), 110480.
- J. Lee, S. Lee, T. Ahmad, S.K. Madhurakkt Perikamana, J. Lee, E.M. Kim, H. Shin, Human adipose-derived stem cell spheroids incorporating platelet-derived growth factor (PDGF) and bio-minerals for vascularized bone tissue engineering, *Biomaterials* 255 (2020), 120192.
- K. Zheng, B. Sui, K. Ilyas, A.R. Boccaccini, Porous bioactive glass micro- and nanospheres with controlled morphology: developments, properties and emerging biomedical applications, *Mater. Horiz.* 8 (2) (2021) 300–335.
- B. Lowe, J.G. Hardy, L.J. Walsh, Optimizing nanohydroxyapatite nanocomposites for bone tissue engineering, *ACS Omega* 5 (1) (2020) 1–9.
- Y. Zhang, N. Kong, Y. Zhang, W. Yang, F. Yan, Size-dependent effects of gold nanoparticles on osteogenic differentiation of human periodontal ligament progenitor cells, *Theranostics* 7 (5) (2017) 1214–1224.
- C. Zhou, S. Liu, J. Li, K. Guo, Q. Yuan, A. Zhong, J. Yang, J. Wang, J. Sun, Z. Wang, Collagen functionalized with graphene oxide enhanced biomimetic mineralization and in situ bone defect repair, *ACS Appl. Mater. Interfaces* 10 (50) (2018) 44080–44091.
- S. Seal, A. Jeyaranjan, C.J. Neal, U. Kumar, T.S. Sakhivel, D.C. Sayle, Engineered defects in cerium oxides: tuning chemical reactivity for biomedical, environmental, & energy applications, *Nanoscale* 12 (13) (2020) 6879–6899.
- A. Ho-Shui-Ling, J. Bolander, L.E. Rustom, A.W. Johnson, F.P. Luyten, C. Picart, Bone regeneration strategies: engineered scaffolds, bioactive molecules and stem cells current stage and future perspectives, *Biomaterials* 180 (2018) 143–162.
- S. Kargozar, F. Baino, S.J. Hoseini, S. Hamzehlou, M. Darroudi, J. Verdi, L. Hasanzadeh, H.W. Kim, M. Mozafari, Biomedical applications of nanoceria: new roles for an old player, *Nanomedicine* 13 (23) (2018) 3051–3069.
- F.Y. Li, Y.P. Qiu, F. Xia, H. Sun, H.W. Liao, A. Xie, J. Lee, P.H. Lin, M. Wei, Y. F. Shao, B. Yang, Q.J. Weng, D.S. Ling, Dual detoxification and inflammatory regulation by ceria nanozymes for drug-induced liver injury therapy, *Nano Today* 35 (2020), 100925.
- S. Zhao, Y.X. Li, Q.Y. Liu, S.R. Li, Y. Cheng, C.Q. Cheng, Z.Y. Sun, Y. Du, C.J. Butch, H. Wei, An orally administered CeO₂@Montmorillonite nanozyme targets inflammation for inflammatory bowel disease therapy, *Adv. Funct. Mater.* 30 (45) (2020), 2004692.
- T. Naganuma, E. Traversa, The effect of cerium valence states at cerium oxide nanoparticle surfaces on cell proliferation, *Biomaterials* 35 (15) (2014) 4441–4453.
- A.S. Karakoti, O. Tsigkou, S. Yue, P.D. Lee, M.M. Stevens, J.R. Jones, S. Seal, Rare earth oxides as nanoadditives in 3-D nanocomposite scaffolds for bone regeneration, *J. Mater. Chem.* 20 (40) (2010) 8912–8919.
- J. Li, J. Wen, B. Li, W. Li, W. Qiao, J. Shen, W. Jin, X. Jiang, K.W.K. Yeung, P. K. Chu, Valence state manipulation of cerium oxide nanoparticles on a titanium surface for modulating cell fate and bone formation, *Adv. Sci.* 5 (2) (2018), 1700678.
- J. Xiang, J. Li, J. He, X. Tang, C. Dou, Z. Cao, B. Yu, C. Zhao, F. Kang, L. Yang, S. Dong, X. Yang, Cerium oxide nanoparticle modified scaffold interface enhances vascularization of bone grafts by activating calcium channel of mesenchymal stem cells, *ACS Appl. Mater. Interfaces* 8 (7) (2016) 4489–4499.
- S. Das, S. Singh, J.M. Dowling, S. Oommen, A. Kumar, T.X.T. Sayle, S. Saraf, C. R. Patra, N.E. Vlahakis, D.C. Sayle, W.T. Self, S. Seal, The induction of angiogenesis by cerium oxide nanoparticles through the modulation of oxygen in intracellular environments, *Biomaterials* 33 (31) (2012) 7746–7755.
- S. Zaichick, V. Zaichick, V. Karandashev, S. Nosenko, Accumulation of rare earth elements in human bone within the lifespan, *Metall* 3 (2) (2011) 186–194.
- P.M. Bartold, S. Gronthos, Standardization of criteria defining periodontal ligament stem cells, *J. Dent. Res.* 96 (5) (2017) 487–490.
- H. Cheng, S. Lin, F. Muhammad, Y.W. Lin, H. Wei, Rationally modulate the oxidase-like activity of nanoceria for self-regulated bioassays, *ACS Sens.* 1 (2016) 1336–1343.
- Y. Liu, Y. Zhang, Q. Liu, Q. Wang, A. Lin, J. Luo, Y. Du, Y.-W. Lin, H. Wei, In vitro measurement of superoxide dismutase-like nanozyme activity: a comparative study, *Analyst* 146 (6) (2021) 1872–1879.
- S. Ren, Y. Yao, H. Zhang, R. Fan, Y. Yu, J. Yang, R. Zhang, C. Liu, W. Sun, L. Miao, Aligned fibers fabricated by near-field electrospinning influence the orientation and differentiation of hPDLSCs for periodontal regeneration, *J. Biomed. Nanotechnol.* 13 (12) (2017) 1725–1734.
- L. Jun, C. Gang, X. Hai, H. Ke, S. Jianfei, L. Mei, Z. Feimin, G. Ning, Pre-vascularization in fibrin Gel/PLGA microsphere scaffolds designed for bone regeneration, *NPG Asia Mater.* 10 (2018) 827–839.
- A. Sculean, D. Nikolidakis, G. Nikou, A. Ivanovic, I.L. Chapple, A. Stavropoulos, Biomaterials for promoting periodontal regeneration in human intrabony defects: a systematic review, *Periodontol.* 2000 68 (1) (2015) 182–216.
- D. Shao, M. Lu, D. Xu, X. Zheng, Y. Pan, Y. Song, J. Xu, M. Li, M. Zhang, J. Li, G. Chi, L. Chen, B. Yang, Carbon dots for tracking and promoting the osteogenic differentiation of mesenchymal stem cells, *Biomater. Sci.* 5 (9) (2017) 1820–1827.
- S. Bose, N. Sarkar, Natural medicinal compounds in bone tissue engineering, *Trends Biotechnol.* 38 (4) (2020) 404–417.
- Y. Xia, X. Fan, H. Yang, L. Li, C. He, C. Cheng, R. Haag, ZnO/Nanocarbons-Modified fibrous scaffolds for stem cell-based osteogenic differentiation, *Small* 16 (38) (2020), e2003010.
- M. Alizadeh, Y. Li, A. Vahid, A. Atee, C. Wen, High strength porous PLA gyroid scaffolds manufactured via fused deposition modeling for tissue-engineering applications, *Smart Mater. Med.* 2 (2021) 15–25.
- C. Xu, X. Qu, Cerium oxide nanoparticle: a remarkably versatile rare earth nanomaterial for biological applications, *NPG Asia Mater.* 6 (3) (2014) 102–108.
- Q. Muhammad, Y. Jang, S.H. Kang, J. Moon, W.J. Kim, H. Park, Modulation of immune responses with nanoparticles and reduction of their immunotoxicity, *Biomater. Sci.* 8 (6) (2020) 1490–1501.
- A.L. Popov, N.R. Popova, Selezneva II, A.Y. Akkizov, V.K. Ivanov, Cerium oxide nanoparticles stimulate proliferation of primary mouse embryonic fibroblasts in vitro, *Mater. Sci. Eng. C Mater. Biol. Appl.* 68 (2016) 406–413.
- I. Celardo, J.Z. Pedersen, E. Traversa, L. Ghibelli, Pharmacological potential of cerium oxide nanoparticles, *Nanoscale* 3 (4) (2011) 1411–1420.
- F. Pagliari, C. Mandoli, G. Forte, E. Magnani, S. Pagliari, G. Nardone, S. Licocchia, M. Minieri, P. Di Nardo, E. Traversa, Cerium oxide nanoparticles protect cardiac progenitor cells from oxidative stress, *ACS Nano* 6 (5) (2012) 3767–3775.
- L. Ma, J. Hu, Y. Cao, Y. Xie, H. Wang, Z. Fan, C. Zhang, J. Wang, C.T. Wu, S. Wang, Maintained properties of aged dental pulp stem cells for superior periodontal tissue regeneration, *Aging Dis.* 10 (4) (2019) 793–806.
- C. Mahapatra, R.K. Singh, J.H. Lee, J. Jung, J.K. Hyun, H.W. Kim, Nano-shape varied cerium oxide nanomaterials rescue human dental stem cells from oxidative

- insult through intracellular or extracellular actions, *Acta Biomater.* 50 (2017) 142–153.
- [50] J.J. Li, N. Kawazoe, G. Chen, Gold nanoparticles with different charge and moiety induce differential cell response on mesenchymal stem cell osteogenesis, *Biomaterials* 54 (2015) 226–236.
- [51] J. Qiu, D. Li, X. Mou, J. Li, W. Guo, S. Wang, X. Yu, B. Ma, S. Zhang, W. Tang, Y. Sang, P.R. Gil, H. Liu, Effects of graphene quantum dots on the self-renewal and differentiation of mesenchymal stem cells, *Adv. Healthc. Mater.* 5 (6) (2016) 702–710.
- [52] B. Lu, D.Y. Zhu, J.H. Yin, H. Xu, C.Q. Zhang, Q.F. Ke, Y.S. Gao, Y.P. Guo, Incorporation of cerium oxide in hollow mesoporous bioglass scaffolds for enhanced bone regeneration by activating the ERK signaling pathway, *Biofabrication* 11 (2) (2019), 025012.
- [53] S.D. Purohit, H. Singh, R. Bhaskar, I. Yadav, C.F. Chou, M.K. Gupta, N.C. Mishra, Gelatin-alginate-cerium oxide nanocomposite scaffold for bone regeneration, *Mater. Sci. Eng. C Mater. Biol. Appl.* 116 (2020), 111111.
- [54] J. Li, F. Kang, X. Gong, Y. Bai, J. Dai, C. Zhao, C. Dou, Z. Cao, M. Liang, R. Dong, H. Jiang, X. Yang, S. Dong, Ceria nanoparticles enhance endochondral ossification-based critical-sized bone defect regeneration by promoting the hypertrophic differentiation of BMSCs via DHX15 activation, *Faseb. J.* 33 (5) (2019) 6378–6389.
- [55] G. Yin, D. Zhao, Y. Ren, L. Zhang, Z. Zhou, Q. Li, A convenient process to fabricate gelatin modified porous PLLA materials with high hydrophilicity and strength, *Biomater. Sci.* 4 (2) (2016) 310–318.
- [56] Z. Xu, Y. Xu, P. Basuthakur, C.R. Patra, S. Ramakrishna, Y. Liu, V. Thomas, H. S. Nanda, Fibro-porous PLLA/gelatin composite membrane doped with cerium oxide nanoparticles as bioactive scaffolds for future angiogenesis, *J. Mater. Chem. B.* 8 (2020) 9110–9120.
- [57] X. Liu, X. He, D. Jin, S. Wu, H. Wang, M. Yin, A. Aldalbahi, M. El-Newehy, X. Mo, J. Wu, A biodegradable multifunctional nanofibrous membrane for periodontal tissue regeneration, *Acta Biomater.* 108 (2020) 207–222.
- [58] H.A. Rather, R. Thakore, R. Singh, D. Jhala, S. Singh, R. Vasita, Antioxidative study of Cerium Oxide nanoparticle functionalised PCL-Gelatin electrospun fibers for wound healing application, *Bioact. Mater.* 3 (2) (2018) 201–211.
- [59] J.H. Lee, D.H. Kim, H.H. Lee, H.W. Kim, Role of nuclear mechanosensitivity in determining cellular responses to forces and biomaterials, *Biomaterials* 197 (2019) 60–71.
- [60] T.C. von Erlach, S. Bertazzo, M.A. Wozniak, C.M. Horejs, S.A. Maynard, S. Attwood, B.K. Robinson, H. Autefage, C. Kallepitis, A. Del Río Hernández, C. S. Chen, S. Goldoni, M.M. Stevens, Cell-geometry-dependent changes in plasma membrane order direct stem cell signalling and fate, *Nat. Mater.* 17 (3) (2018) 237–242.